Journal of Inflammation Research

Dovepress
Taylor & Francis Group

Open Access Full Text Article

ORIGINAL RESEARCH

Machine Learning-Based Identification and Experimental Validation of Hub Ferroptosis-Related Cuproptosis Genes in Lupus Nephritis

Su Zhang[1,2,*], Weitao Hu[3,*], Yifang Zhang[1], Chunyan Huang[4], Ziqiong He[1], Jing Xu[1], Shihong Lin[1], Baoya Yang[1], Xiaoqing Chen[1,2]

[1]The Second Clinical College of Fujian Medical University, Quanzhou, People's Republic of China; [2]Department of Rheumatology, The Second Affiliated Hospital of Fujian Medical University, Quanzhou, People's Republic of China; [3]Department of Gastroenterology, The Second Affiliated Hospital of Fujian Medical University, Quanzhou, People's Republic of China; [4]Department of General Practice, The Second Affiliated Hospital of Fujian Medical University, Quanzhou, People's Republic of China

*These authors have contributed equally to this work

Correspondence: Xiaoqing Chen, Email chenxiaoqing202203@163.com

Background: The role of ferroptosis and cuproptosis in lupus nephritis (LN) is unclear. The aim of this study was to explore the expression and effects of ferroptosis-related cuproptosis genes (FRCGs) in LN using bioinformatics and experimental validation.

Methods: The LN-related datasets GSE112943 and GSE32591 were downloaded from the GEO database. We collected 834 ferroptosis-related genes and 1046 cuproptosis-related genes. Weighted gene co-expression network analysis (WGCNA) and machine learning algorithms identified hub FRCGs in the LN. We then analyzed the relationship of hub FRCGs with immune infiltration and clinical traits. Finally, we validated the expression of the hub FRCGs in vivo and in vitro.

Results: A total of 31 differentially expressed FRCGs (DE-FRCGs) in the LN were screened, which were mainly involved in the response to metal ions and oxidative stress. And they were engaged in autophagy-animal signaling pathway. Machine learning identified two hub FRCGs (*JUN* and *ZFP36*). Public datasets, clinical samples, in vivo and in vitro experiments confirmed that hub FRCGs expression was reduced in the LN group compared to control group. Immune infiltration analysis displayed that monocytes and macrophages were the major infiltrating cells in LN kidneys. In LN, hub genes were negatively correlated with macrophages and monocytes.

Conclusion: This study elucidates the contribution of ferroptosis-related cuproptosis genes to the onset and progression of LN. *JUN* and *ZFP36* were potentially effective biomarkers of LN and may be potential targets for LN therapy in the future.

Keywords: ferroptosis, cuproptosis, lupus nephritis, machine learning, immune infiltration

Introduction

Lupus nephritis (LN) is one of the common and serious complications of systemic lupus erythematosus (SLE). It is typically characterized by decreased glomerular filtration rate, proteinuria and elevated serum creatinine levels.[1,2] The pathogenesis of LN is intricate, and is currently thought to be the outcome of a multifactorial combination of genetic, endocrine, and environmental factors.[3] At present, the conventional treatment of LN relies mainly on drugs such as steroid hormones and some immunosuppressants.[3] However, 10–20% of patients are still progressing to end-stage renal disease.[4] In addition, the diverse symptoms of LN provide difficulties in the diagnosis of LN. Therefore, continued exploration of novel biomarkers and potential therapeutic targets for LN remains a promising direction.

Ferroptosis is a mode of cell death characterized by iron imbalance, lipid peroxidation, and dysregulation of antioxidant systems.[5] This cell death plays an important role in the pathogenesis of various diseases, including tumor development, neurological, cardiovascular, and intestinal system diseases.[6] The importance of iron as one of the essential elements in human body has been reported in maintaining immune infiltration. Oxides catalyzed by ferroptosis can increase immune cell infiltration, leading to the development of renal inflammation and renal failure.[7] In addition, there

Received: 6 March 2025
Accepted: 11 August 2025
Published: 18 August 2025

are many studies on ferroptosis-related genes and their role in LN. The ferroptosis of neutrophils causes SLE.[8] Marks reported that LN presents with renal iron accumulation and that the application of ferroptosis inhibitors slows proteinuria levels.[9] However, few studies have been conducted to link ferroptosis to cuproptosis in LN.

Crucially, metal ions, particularly iron and copper, share interconnected metabolic pathways and can both drive oxidative stress and regulated cell death. Cuproptosis is a novel mode of cell death distinct from ferroptosis, disulfidptosis, and apoptosis first proposed in 2022. Cuproptosis occurs when intracellular copper overload triggers aggregation of mitochondrial lipidation proteins and destabilization of Fe-S cluster proteins.[10] While cuproptosis has been rapidly explored in tumor, cardiovascular, and neurological diseases,[11,12] its potential role in LN, and crucially its interplay with the established pathway of ferroptosis, remains entirely unexplored. This gap is significant given the shared triggers of metal ion dyshomeostasis and oxidative stress in both pathways, and the established role of oxidative stress and immune dysregulation in LN pathogenesis. Emerging evidence even suggests potential crosstalk, such as copper promoting ferroptosis via autophagic degradation of GPX4.[13]

Therefore, to investigate the potential convergence of two metal ion-dependent cell death pathways in LN, we defined a novel concept: Ferroptosis-Related Cuproptosis Genes (FRCGs). We hypothesized that genes intersecting both ferroptosis and cuproptosis pathways might be critically dysregulated in LN, contributing to renal injury through shared mechanisms involving metal ion toxicity and oxidative stress. This study represents the first systematic investigation into the combined role of ferroptosis and cuproptosis in LN.

While previous studies have identified individual biomarkers for LN, the application of machine learning methods in identifying hub genes that intersect both ferroptosis and cuproptosis pathways provides a novel approach to discovering biomarkers with greater predictive accuracy. This integration is crucial for improving the diagnostic and prognostic potential in LN, offering new insights into the disease mechanisms.

In this study, bioinformatics analysis and machine learning methods were integrated to screen the hub FRCGs in LN. A nomogram was constructed for diagnostic prediction, validated with an independent LN dataset. The potential of the identified biomarkers was further investigated and confirmed through in vitro and in vivo experiments. Our aim was to identify novel biomarkers for LN and provide new insights into the pathogenesis involving dysregulated metal ion-dependent cell death.

Materials and Methods

Acquisition of Datasets and Screening of Differentially Expressed Genes

In this study, the LN datasets were obtained from the GEO database (https://www.ncbi.nlm.nih.gov/geo/),[14] where GSE112943 (GPL10558) (training cohort) included the kidney samples of 14 LN patients and 7 normal controls (NC). GSE32591 (GPL14663) (validating cohort) contained the 32 glomerular and 32 tubular samples from LN patients, 14 glomerular and 15 tubular samples from NC. Firstly, we assessed and corrected for batch effects during the normalization process. Specifically, we used the "ComBat" method from the sva R package to adjust for any batch-related variation in the gene expression data. The training cohort was then screened for differentially expressed genes (DEGs) with the "limma" package of R.[15] The screening criteria for DEGs: $|\log2FC|>0.5$ and an adjusted $P<0.05$. The details of the datasets covered in this study are presented in Table 1.

Table 1 The Details of the Datasets Included in This Study

Dataset	Platform	Species	Sources	Number of Cases and Controls	Type of Cohortts
GSE112943 GSE32591	GPL10558 GPL14663	*Homo sapiens*	Kidney Glomeruli and tubules	12 LN/7 NC 64 LN/29 NC	Training Validating

Abbreviations: LN, lupus nephritis; NC, normal control.

Weighted Gene Co-Expression Network Analysis

In order to obtain the modules and their genes that are most closely related to the clinical traits of the LN, the training set was subjected to weighted gene co-expression network analysis (WGCNA). The picksoftThreshold function was first utilized to determine the optimal soft threshold. Subsequently, modules with distances less than 0.3 were merged. Each module including at least 30 genes. Meaningless genes were incorporated into grey module. In addition, Pearson test elucidated the correlation between each module and clinical traits. Finally, scatter plots showed the correlation of module membership (MM) and gene significance (GS) with LN. The above analysis were realized with the "WGCNA" package of R.[16]

Identification of Differentially Expressed Ferroptosis-Related Cuproptosis Genes in LN

The 834 ferroptosis-related genes (FRGs) were obtained from the FerrDb V2 database (http://www.zhounan.org/ferrdb/).[17] A total of 1046 cuproptosis-related genes (CRGs) were obtained from GeneCards,[18] MsigDB databases[19] and previous study (PMID:35298263).[20] The DEGs, WGCNA, FRGs, and CRGs were taken to intersect to obtain the differentially expressed ferroptosis-related cuproptosis genes (DE-FRCGs) in LN.

Protein-Protein Interaction Network Construction and Functional Enrichment Analysis of DE-FRCGs

The DE-FRCGs were uploaded to the STRING database (https://cn.string-db.org/),[21] requiring a minimum score of 0.4 to obtain the protein-protein interaction network, and the PPI network was further visualized by Cytoscape (version 3.9.1).[22] The DE-FRCGs were then analyzed for Gene Ontology (GO) and Kyoto Encyclopedia of Genes and Genomes (KEGG) enrichment using the "clusterprofiler" package of R to understand their biological functions.[23] Among the GO enrichments include biological processes (BP), cellular components (CC), and molecular functions (MF).

Identification of Hub FRCGs and Construction of Nomogram

In order to further screen the hub FRCGs in the LN, we first conducted least absolute shrinkage and selection operator (LASSO) regression analyses on the DE-FRCGs using the "glnmet" package.[24] LASSO regression employed the parameter λ to control the complexity of the model. The optimal value of λ was selected through 10-fold cross-validation, where we calculated the mean squared error (MSE) for each value of λ. The λ value that minimized the MSE was chosen as the best tuning parameter. To further ensure model stability, we also applied the 1SE rule, where the largest λ within one standard error of the minimum MSE was considered an alternative optimal value. This process ensured that the model not only fits the data well but is also robust and less likely to overfit. Then we applied the "randomforest" and "e1071" packages to perform random forest (RF) and support vector machine-recursive feature elimination (SVM-RFE) analysis.[25,26] Characteristic importance scores for each gene were determined by random forest model, with the top 10 genes were selected based on their importance values. In the model, "ntrees = 500" was selected as the default value to balance model accuracy and computational efficiency. Furthermore, feature importance was calculated using the Gini index method, chosen to assess the contribution of each gene to the model. Subsequently, the intersection of the signature genes screened by the three machine learning methods was taken to obtain the hub FRCGs in the LN. Finally, a nomogram was constructed, and the "pROC" package was utilized to generate the receiver operating characteristic (ROC) curve.[27] An area under the curve (AUC) approaching 1 indicates a higher diagnostic performance of the model.

External Dataset Validation of Hub Genes

We then further explored the expression levels of the hub genes in GSE32591. Finally, their ROC curves were drawn to further assess their ability to serve as biomarkers for distinguishing LN from NC.

Clinical Samples Validate Hub Genes Expression

Collection of Samples

Peripheral blood samples and paraffin sections were collected from 20 patients diagnosed with lupus nephritis by pathologic puncture from January 2024 to January 2025 at the Second Affiliated Hospital of Fujian Medical University. The control group of peripheral blood was selected from healthy people who excluded hepatitis B/C, diabetes mellitus, malignant tumors, pathogenic infection, cardiovascular diseases, other renal diseases, chronic liver diseases or other types of autoimmune diseases. We also collected gender, age, and relevant clinical and laboratory indicators for all volunteers (Table 2). Control paraffin-embedded kidney tissue sections were derived from histologically normal renal parenchyma in paracancerous tissues. These tissues were located ≥5 cm from the tumor margin and obtained from nephrectomy specimens of renal cell carcinoma patients.

Extraction of Peripheral Blood Mononuclear Cells

Erythrocyte lysate (C3702) and lymphocyte isolate (C0025) were purchased from Beyotime (Shanghai, China). Briefly, an equal volume of PBS solution is added to whole blood followed by lymphocyte isolate. A small amount of erythrocyte lysate was added after centrifugation. Centrifuge again, and take the supernatant from the tube for cell counting and freeze it for subsequent RNA extraction.

Real-Time Quantitative Polymerase Chain Reaction (RT-qPCR)

The RNA extraction kit (R0027) was purchased from Bryotime (Shanghai, China). Reverse transcription reagents were purchased from Takara (Japan). Follow the appropriate instructions to extract cDNA. Finally, ABI PRISM 7500 PCR instrument (AppliedBiosystems, United States of America) was used to amplify the target gene. The details of the procedure and experimental conditions can be referred to our previous study.[28] The primers used in this section are exhibited in Table 3.

Immunohistochemical (IHC) Staining of the Kidneys

The paraffin sections were deparaffinized and processed for antigen repair ((pH 6.0, 95°C, 15 min)). Rabbit anti-JUN antibody (24909-1-AP, proteintech, 1:200) and rabbit anti-ZFP36 antibody (12737-1-AP, proteintech, 1:200) were then applied and incubated with the sections overnight at 4°C refrigerators. Confinement and incubation of the corresponding

Table 2 Clinical Traits of LN Patients and Normal Controls

Clinical Traits*	LN (n = 20)	Normal Controls (n = 22)
Sex, male/female	2/18	2/20
Age (year)	34.67 ± 16.29	33.55 ± 10.19
Duration (year)	9.73 ± 6.37	–
ANA (Positive)	19 (20)	–
Anti-dsDNA antibody (Positive)	16 (20)	–
Lupus anticoagulant (Positive)	12 (20)	–
Leukocyte (10^9/L)	5.53 ± 1.71	–
Platelets (10^9/L)	185.35 ± 92.24	–
CRP (mg/L)	10.01 ± 7.23	–
ESR (mm/h)	20.6 ± 14.79	–
C3 (g/L)	0.73 ± 0.45	–
C4 (g/L)	0.1 ± 0.05	–
IgG (g/L)	15.24 ± 8.15	–
IgA (g/L)	2.64 ± 1.7	–
IgM (g/L)	0.8 ± 0.67	–
Serum creatinine (μmol/L)	73.91 ± 58.26	–
24h urine protein (Positive)	12 (20)	–

Abbreviations: *LN, lupus nephritis; ANA, antinuclear antibody; Anti-dsDNA antibody, anti-double stranded deoxyribonucleic acid antibody; CRP, C-reactive protein; ESR, erythrocyte sedimentation rate; C3/C4, complement 3/complement 4; Igs, immunoglobulins.

Table 3 Primer Sequences of Involved in This Study

Gene symbol	Forward Primer (5' → 3')	Reverse Primer (5' → 3')
B-actin-human	AGGTCTTTGCGGATGTCCACGT	AGGTCTTTGCGGATGTCCACGT
JUN-human	TCCAAGTGCCGAAAAAGGAAG	CGAGTTCTGAGCTTTCAAGGT
ZFP36-human	GACTGAGCTATGTCGGACCTT	GAGTTCCGTCTTGTATTTGGGG
B-actin-mouse	GGCTGTATTCCCCTCCATCG	CCAGTTGGTAACAATGCCATGT
JUN-mouse	CCTTCTACGACGATGCCCTC	GGTTCAAGGTCATGCTCTGTTT
ZFP36-mouse	CCACCTCCTCTCGATACAAGA	GCTTGGCGAAGTTCACCCA
ACSL4-mouse	CTCACCATTATATTGCTGCCTGT	TCTCTTTGCCATAGCGTTTTTCT
LIAS-mouse	CCTGGGGTCCCGGATATTTG	GAAGGTCTGGTCCATTATGCAA
SLC7A11-mouse	GGCACCGTCATCGGATCAG	CTCCACAGGCAGACCAGAAAA

secondary antibodies were performed the next day. After that, DAB chromogen and hematoxylin counterstaining were performed. Finally, mounting treatment was conducted, and the samples were observed under a microscope.

Animal Experimentation

Animal Selection

MRL/lpr mouse has been applied in several studies as a commonly used lupus mouse model,[29] and female C57BL/6 mice of the same week were the normal controls (NC). The urine protein and plasma anti-dsDNA antibody of C57BL/6 mice and MRL/lpr mice was measured weekly from 16 weeks of age, and the mice were killed at 20 weeks of age after modeling. Spleen index and perirenal lymph node index were measured. The mice were executed by intravenous injection of amobarbital at the end of the experiment. The above mice were purchased from Shanghai SLAC Laboratory Animal Corporation.

Masson Staining

Masson staining involved fixing the tissue, followed by dehydration and clearing. The tissue was stained with Weigert's hematoxylin (8min) for the nuclei, Biebrich Scarlet-Acid Fuchsin (5min) for the cytoplasm and muscle fibers, and Aniline Blue for collagen fibers (2min). The tissues were then differentiated with phosphotungstic acid (1min per wash), rehydrated, dehydrated again, and cleared. Finally, the tissue is mounted with a cover slip. The result shows cell nuclei in blue-black, cytoplasm and muscle fibers in red, and collagen fibers in blue.

Periodic aid-Shiff (PAS) Staining

Firstly, the tissue sections were de-graphitized and hydrated. Then, sugars were oxidized to aldehydes using periodic acids. These aldehydes were then stained using Schiff's reagent to give a pink to purple color. After rinsing, the tissue was counterstained with hematoxylin to highlight the nuclei. Finally, the sections were dehydrated, washed and mounted for microscopic examination.

Immunofluorescence (IF) Staining

Tissue sections were deparaffinized and hydrated by removing paraffin by immersion in xylene and graded alcohol, followed by hydration of the sections to an aqueous solution. Subsequently, the ability of the antibody to enter the cells was enhanced by treatment with a permeabilizing agent (Triton X-100). Primary antibodies (C3: ab97462, abcam, 1:1000; IgG: ab172730 abcam, 1:1000) against the target antigens were then added and incubated at 4°C overnight. Following this, unbound antibody was removed, secondary antibody with fluorescent dye was added, and incubation is continued for 1h at room temperature. Finally, the sections were washed to remove excess secondary antibody and sealed with fluorescent medium, and the fluorescent signal of the target antigen in the sections was observed under a fluorescence microscope.

IHC Staining

The levels of ferroptosis and cuproptosis were further evaluated by detecting the protein levels of the ferroptosis marker genes TfR1 (Transferrin receptor protein 1) and 4-HNE (4-Hydroxynonenal) as well as the cuproptosis marker gene

FDX1 (Ferredoxin 1) in each group of mice. The source and dilution concentrations of primary antibodies were as follows: TfR1 (1:200, AF5343, affinity), 4-HNE (1:200, GTX01087, gene tex) and FDX1 (1:500, 12,592-1-AP, proteintech). The Steps Were as Described Previously.

Cell Culture and Treatment

Mouse glomerular mesangial cells SV40-MES-13 were purchased from Wuhan Procell Life Science and Technology Co. The cells were cultured at 37°C with 5% CO2 using specialized medium (CM-M057, procell). Cell models were constructed using 5ug/ml concentration of LPS intervening cells for 6h.[30]

Western Blotting

The proteins were extracted from kidney tissues or cells and then quantified by determining the protein concentration using the BCA protein kit (A55864, thermofisher). Afterwards, proteins were separated by 8%, 10% or 12% SDS-PAGE (30min at 80V for stacking gel and 90min at 120V for separating gel) and transferred to polyvinylidene fluoride membranes. The membranes were closed by immersion in 5% skim milk powder for 2h and then placed in a 4°C refrigerator for overnight incubation with primary antibodies (GAPDH: 1:50000, 60004-1-Ig, proteintech; JUN: 1:1000, 24909-1-AP, proteintech; ZFP36: 1:1000, 12737-1-AP, proteintech; LIAS: 1:2000, 11577-1-AP, proteintech; ACSL4: 1:10000, ab155282, abcam; SLC7A11: 1:1000, 12691, CST). The next day, the membranes were incubated with the corresponding secondary antibodies (1:10000, SA00001-2, proteintech) for 1h at room temperature. Subsequently, the membrane was immersed in enhanced chemiluminescence working solution (BL523B, biosharp, China) for 30s. Finally, imaging acquisition was performed under enhanced chemiluminescence immersion.

Real-Time Quantitative Polymerase Chain Reaction (RT-qPCR)

The Steps Were as Described Previously. The Primers Were Displayed in Table 3.

Detection of Oxide Species

MDA (S0131S, Beyotime, Shanghai, China), GSH (A006-2-1, Jiancheng Bioengineering Institute, Nanjing, China), ROS (S0033S, Beyotime, Shanghai, China) and Fe^{2+} (HY-K0322, MedChemExpress, United States) test kits were detected MDA, GSH, ROS and Fe^{2+} levels in cells. Operating according to the manufacturer's instructions.

Relationship Between Hub Genes and Clinical Traits of LN

Based on the Nephroseq v5 database, the expression levels of hub genes were analyzed. To evaluate the clinical relevance of hub genes, we analyzed their correlation with key renal function parameters in LN patients using Nephroseq v5 data. These parameters are fundamental diagnostic and prognostic markers in nephrology. Glomerular filtration rate (GFR) reflects the filtration capacity of the kidneys. In LN patients, the GFR is usually reduced due to impaired glomerular function. Proteinuria is used to quantify the amount of protein lost in the urine and reflects the impaired glomerular barrier. While serum creatinine (Scr) reflects renal excretory function, an elevated Scr indicates reduced renal clearance in LN. Therefore, we then performed a Pearson test to explore the correlation between the hub genes and the above three metrics.

Immune Infiltration Analysis

Cibersort (https://cibersortx.stanford.edu/)[31] was performed to compute scores for 22 immune infiltrating cell types in LN and NC kidney samples, repeated 1000 times. In addition, Pearson test was performed to explore the correlation between the hub genes and the immune infiltrating cells, and the significance level was set at $P < 0.05$ with a Pearson correlation coefficient (R) > 0.35, indicating that there is a correlation between them.

Ethics Statement

The study was approved by the Ethics Committee of the Second Affiliated Hospital of Fujian Medical University under the ethical approval number [2024 (082)] and followed the Declaration of Helsinki. Written informed consent was signed

by each study participant. The animal study protocol was approved by the Institutional Animal Care and Use Committee of Fujian Medical University and followed the standards of the National Institutes of Health Guide for the Care and Use of Laboratory Animals (SYSU-IACUC-2022-001210).

Statistical Analysis

All analyses were conducted using R software (version 4.3.3) and Graphpad prisim (version 10.1.2). Pearson test was utilized to explore the correlation between hub genes and immune infiltrating cells, and $P < 0.05$ was deemed statistically significant. A flowchart of the study is presented in Figure 1.

Results

Identification of DEGs

The median gene expression per sample in the normalized dataset remained consistent, indicating that potential batch effects were eliminated, facilitating subsequent studies (Figure 2A and B). A total of 12520 DEGs (Supplementary material) were screened in the LN and NC groups, including 7151 up-regulated genes and 5369 down-regulated genes (Figure 2C and D).

Identification of Key Gene Modules

In order to obtain key genes highly correlated with the clinical traits of LN, WGCNA was conducted on GSE112943. The mean connectivity was best when the soft threshold was 12 (R-square = 0.8) (Figure 2E). The 21 co-expression modules were obtained by combining the proximity modules (Figure 2F). The correlation between each module and the LN clinical traits was then calculated. The results showed that the greenyellow (cor = 0.83, P = 4e-06) and brown (cor = −0.86, P = 6e-07) modules were highly correlated with clinical phenotypes (Figure 2G and H).

Acquisition and Functional Enrichment Analysis of DE-FRCGs

The DEGs, WGCNAs, FRGs and CRGs were taken to intersect to obtain the 31 DE-FRCGs in the LN (Figure 3A). They formed a PPI network of 25 nodes and 68 edges, suggesting that they are involved in the same biological process (Figure 3B). GO analysis of 31 DE-FRCGs showed that they were mainly involved in the response to metal ion and the cellular response to oxidative stress (Figure 3C and D). KEGG enrichment revealed that the main pathway was

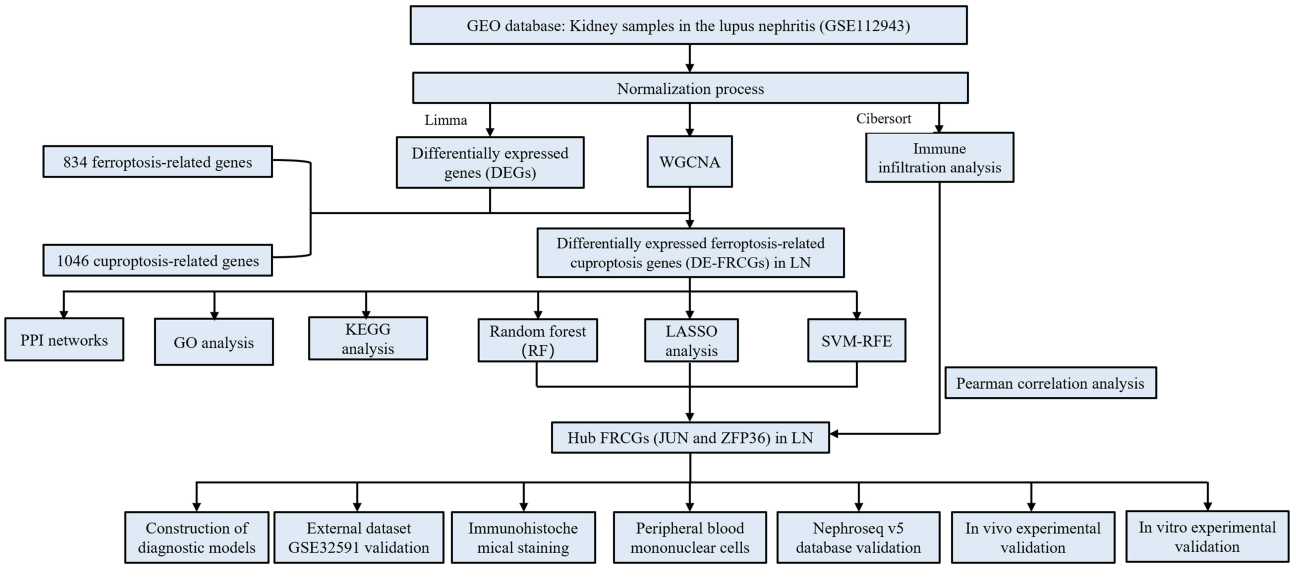

Figure 1 Flowchart of this study.

https://doi.org/10.2147/JIR.S526572

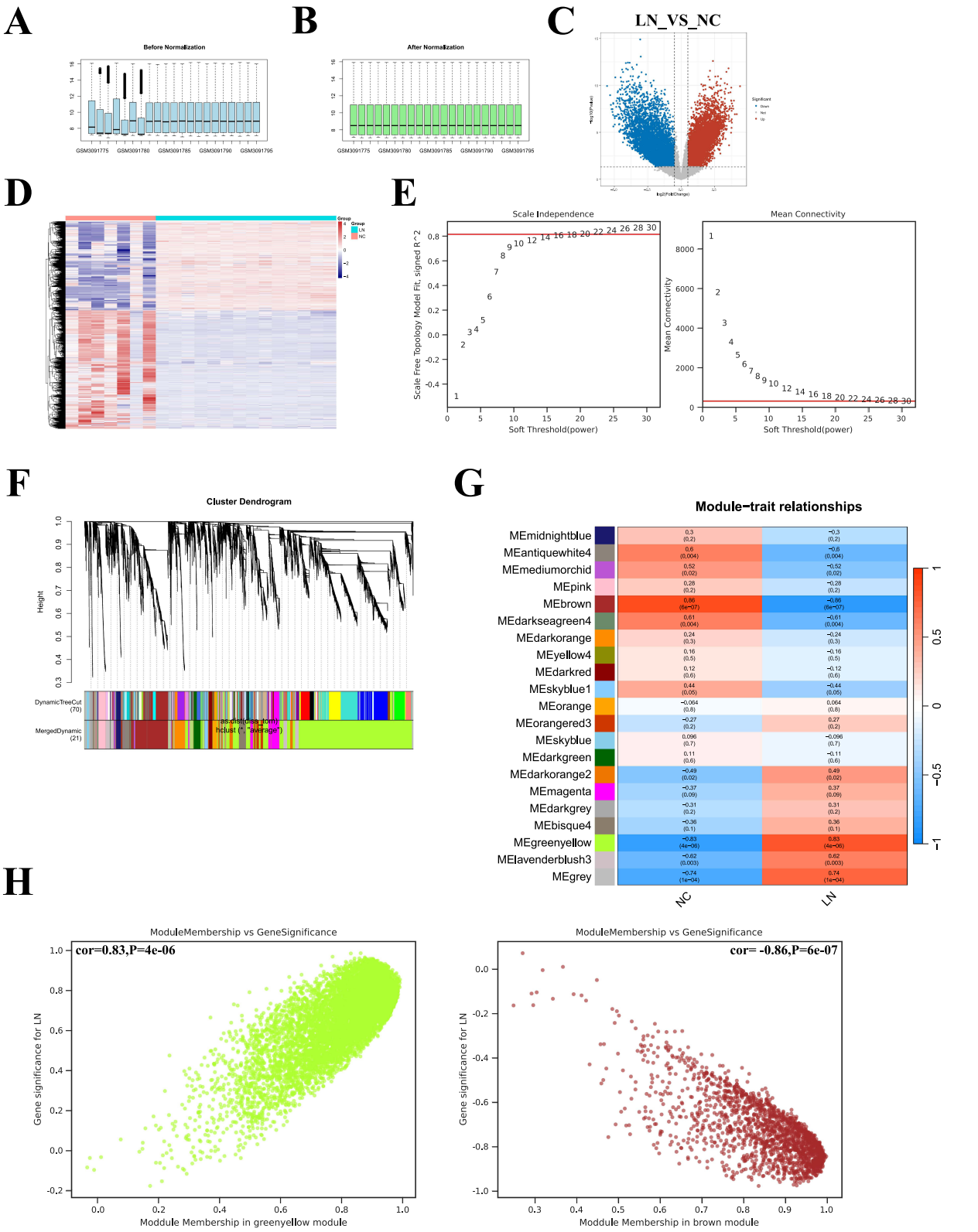

Figure 2 Identification of DEGs and WGCNA. (**A** and **B**) Normalization of GSE12943. (**C**) The volcano plot displayed the DEGs. Red represents upregulated genes, while blue represents downregulated genes. (**D**) The heatmap showed the distribution of DEGs in LN and NC groups. (**E**) The soft threshold power (left) and mean connectivity (right) of the WGCNA. (**F**) Cluster dendrogram for WGCNA analysis. (**G**) The heatmap showed the relationship between the modules and clinical traits, particularly LN and NC. (**H**) The scatterplot revealed the correlation of greenyellow and brown module members (MM) with gene significance (GS).

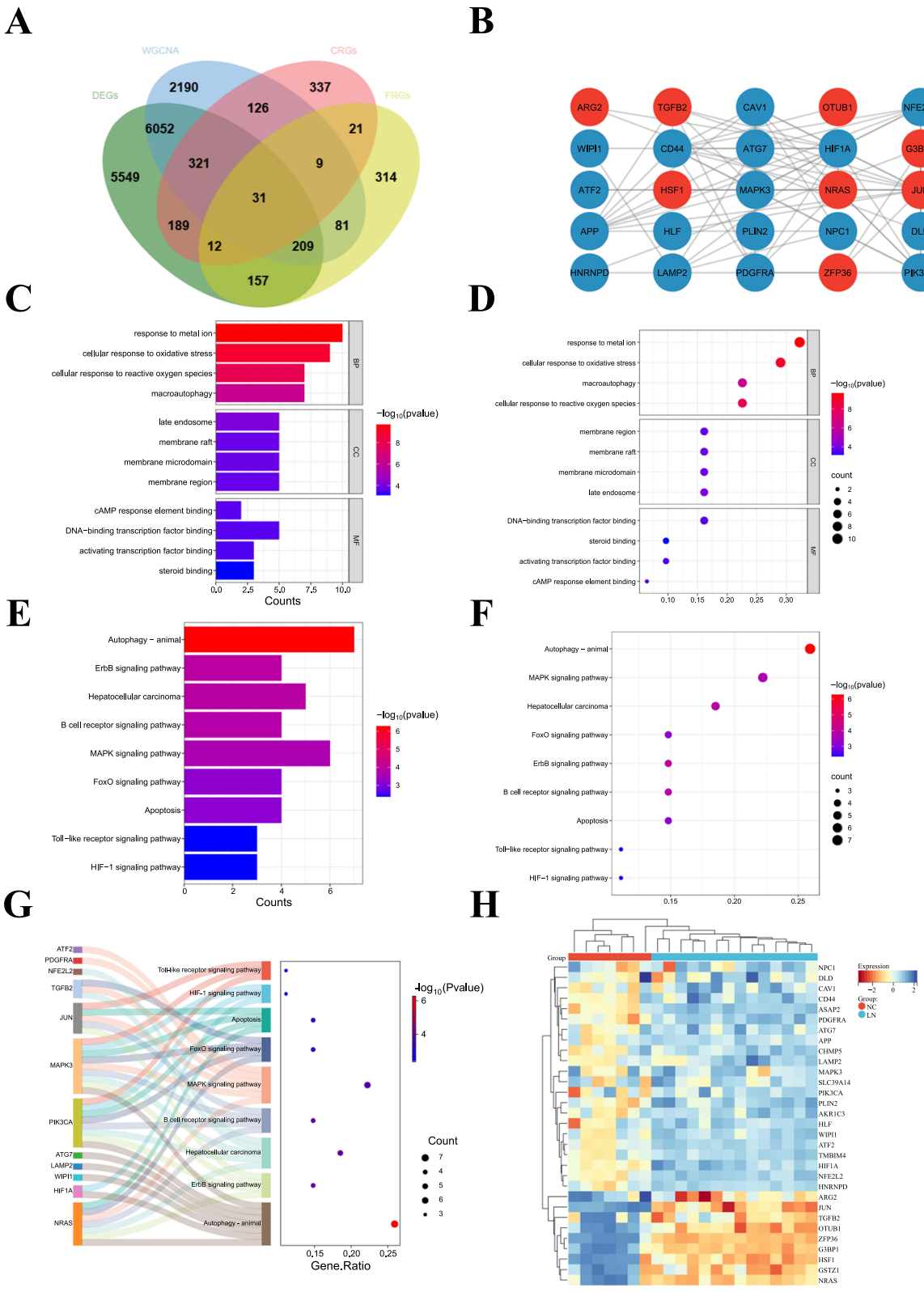

Figure 3 Acquisition and functional analysis of DE-FRCGs in LN. (**A**) The venn plot of DEGs, WGCNA, FRGs and CRGs. (**B**) The PPI network of DE-FRGs. Blue represents upregulated genes, while red represents downregulated genes. (**C**): Bar plot of GO enrichment analysis. (**D**): Bubble plot of GO enrichment analysis. (**E**) Bar plot of KEGG enrichment analysis. (**F**): Bubble plot of KEGG enrichment analysis. (**G**) Sankey diagram of KEGG enrichment analysis. (**H**) The heatmap showed the distribution of DE-FRCGs in LN and NC groups.

https://doi.org/10.2147/JIR.S526572

"autophagy-animal" (Figure 3E–G). In addition, the heatmap displayed the distribution of DE-FRCGs in the LN and NC groups (Figure 3H).

Identification of Hub DE-FRCGs and Construction of a Model Based on Machine Learning

The hub FRCGs in LN were further identified using three machine learning methods. LASSO regression analysis identified 5 genes (Figure 4A and B). RF got the top 10 genes in terms of gene importance (Figure 4C). In addition, SVM-RFE obtained 13 genes (Figure 4D). Eventually, two hub genes were identified, including *JUN* and *ZFP36* (Figure 4E). A nomogram was then plotted for predicting the risk of LN (Figure 4F). We calculated the AUC of ROC curve, which showed AUC=1, suggesting a convincing diagnostic performance of the model (Figure 4G). The violin plots displayed decreased expression of *JUN* and *ZFP36* in the LN (Figure 4H).

External Datasets and Clinical Samples Validation of Hub Genes

We verified the expression of the hub genes in GSE32591. Interestingly, the expression of the hub genes was significantly lower in the LN than in the NC groups, both in glomerular and tubular samples (Figure 5A and B). Then the ROC curves based on the GSE32591 expression matrix were plotted, and the AUCs were all greater than 0.5, which indicated that the prediction accuracy of the hub genes was high (Figure 5C). The results of RT-qPCR of PBMC and IHC staining of paraffin sections of kidney tissues also supported our analysis (Figure 5D–F).

In Vivo Experiments Verified the Expression of the Hub Genes

MRL/lpr mice had significantly higher 24h urinary protein levels, plasma anti-ds-DNA antibody levels, spleen index, and perirenal lymph node index than C57BL/6 mice (Figure 6A–D). IF staining also showed that the levels of C3 and IgG deposition in the kidneys of MRL/lpr mice were also significantly more than those of C57BL/6 mice (Figure 6E). Masson staining suggested that fibrosis was more severe in MRL/lpr mice than in C57BL/6 mice (Figure 6F). In addition, PAS staining revealed infiltration of inflammatory cells and proliferation of mesangial cells in the kidneys of MRL/lpr mice (Figure 6F). These results all suggested that the LN mice model was successfully constructed.

The results of RT-qPCR showed that the expression of *JUN* and *ZFP36* was significantly higher in the MRL/lpr mice than in the C57BL/6 mice (Figure 6G). In addition, the expression of ACSL4 (a key promoter gene of ferroptosis) and LIAS (a key promoter gene of cuproptosis) were also found to be significantly upregulated in the MRL/lpr mice group, whereas SLC7A11 (a common protective gene for ferroptosis and cuproptosis) was significantly downregulated (Figure 6H and I). We also observed significantly higher protein levels of the TfR1, 4-HNE and FDX1 in MRL/lpr mice than in control mice. All these results strongly suggested that excessive ferroptosis and cuproptosis occurred in LN mice.

In Vitro Experiments Verified the Expression of Hub Genes and Elevated Levels of Ferroptosis and Cuproptosis

We then detected the levels of malondialdehyde (MDA), glutathione (GSH), Fe^{2+} and reactive oxygen species (ROS) in both groups of cells. The results revealed that MDA, Fe^{2+} and ROS levels were significantly higher in LPS constructed LN cells, while GSH levels were significantly lower than in the control group (Figure 7A–C). In addition, LPS intervention significantly reduced the levels of JUN, ZFP36 and SLC7A11, while significantly increasing the levels of ACSL4 and LIAS (Figure 7D and E). These were consistent with the previous analysis.

Correlation of Hub Genes with Clinical Traits

Coincidentally, *ZFP36* and *JUN* expression levels were also found to be decreased in LN patients (Figure 8A and B). Intriguingly, *ZFP36* was found to be positively correlated with GFR (R=0.55, P=0.0082) (Figure 8C). Unexpectedly, we observed that the expression of *JUN* was negatively correlated with GFR (R=−0.6, P=2.2e-05) (Figure 8D). However, the expression of *ZFP36* and *JUN* was negatively correlated with both proteinuria (R= −0.96, P=0.04 and R= −0.83,

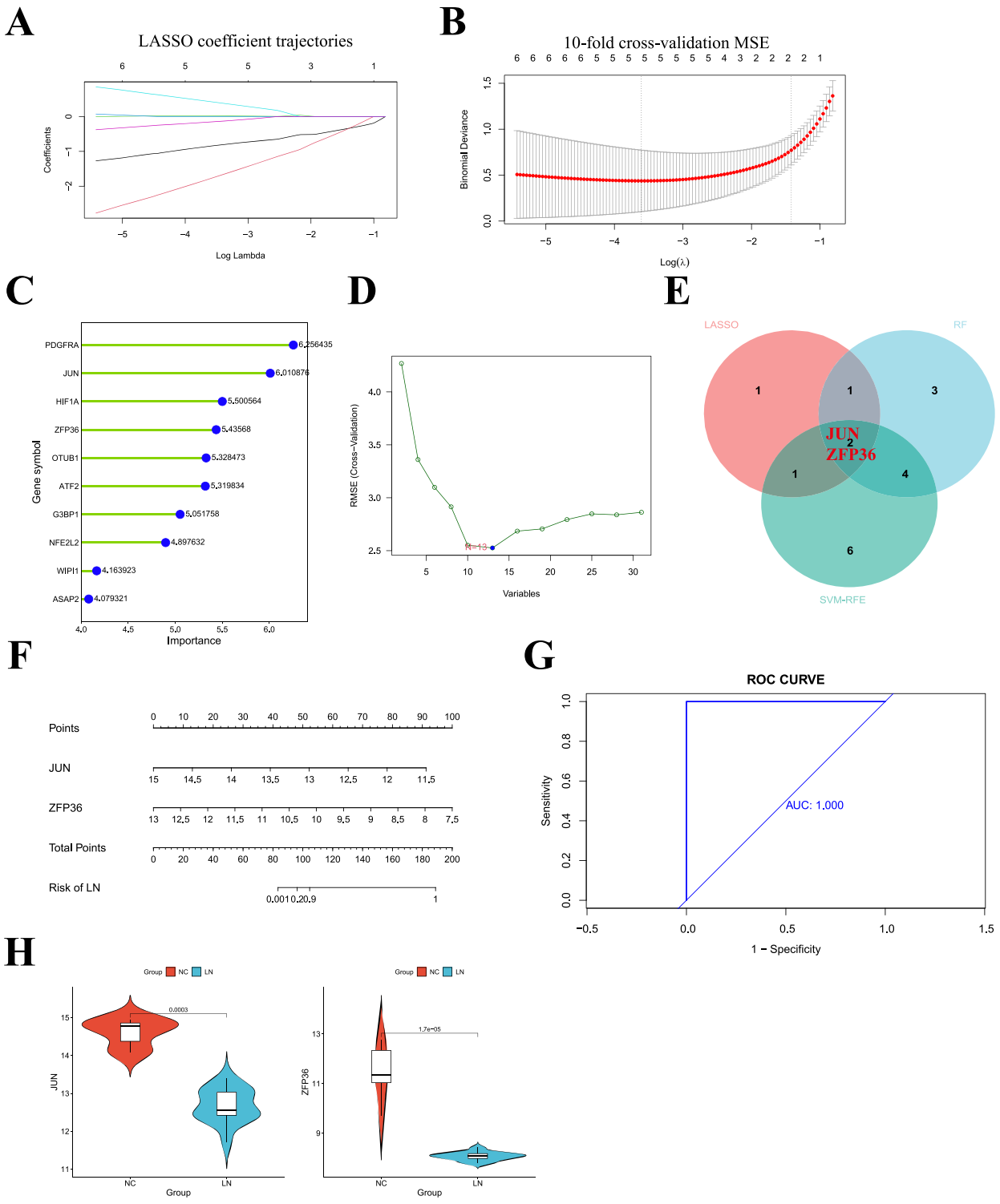

Figure 4 Identification of hub FRCGs in LN. (**A**): Path diagram of LASSO regression coefficients for DE-FRCGs in the training set. X-axis label: Log(λ), Y-axis label: Coefficient values. (**B**): LASSO regression cross-validation curves. A 10-fold cross-validation was used in the training set to determine the optimal λ value. (**C**): The lollipop plot illustrated the relative importance of genes in the random forest model in the training set. (**D**): SVM-RFEs algorithm to screen signature genes. (**E**): The venn diagram showed hub FRCGs. (**F, G**) The nomogram and ROC curve plotted based on the training set. (**H**) The violin plots showed the expression of the hub genes in GSE112943.

https://doi.org/10.2147/JIR.S526572

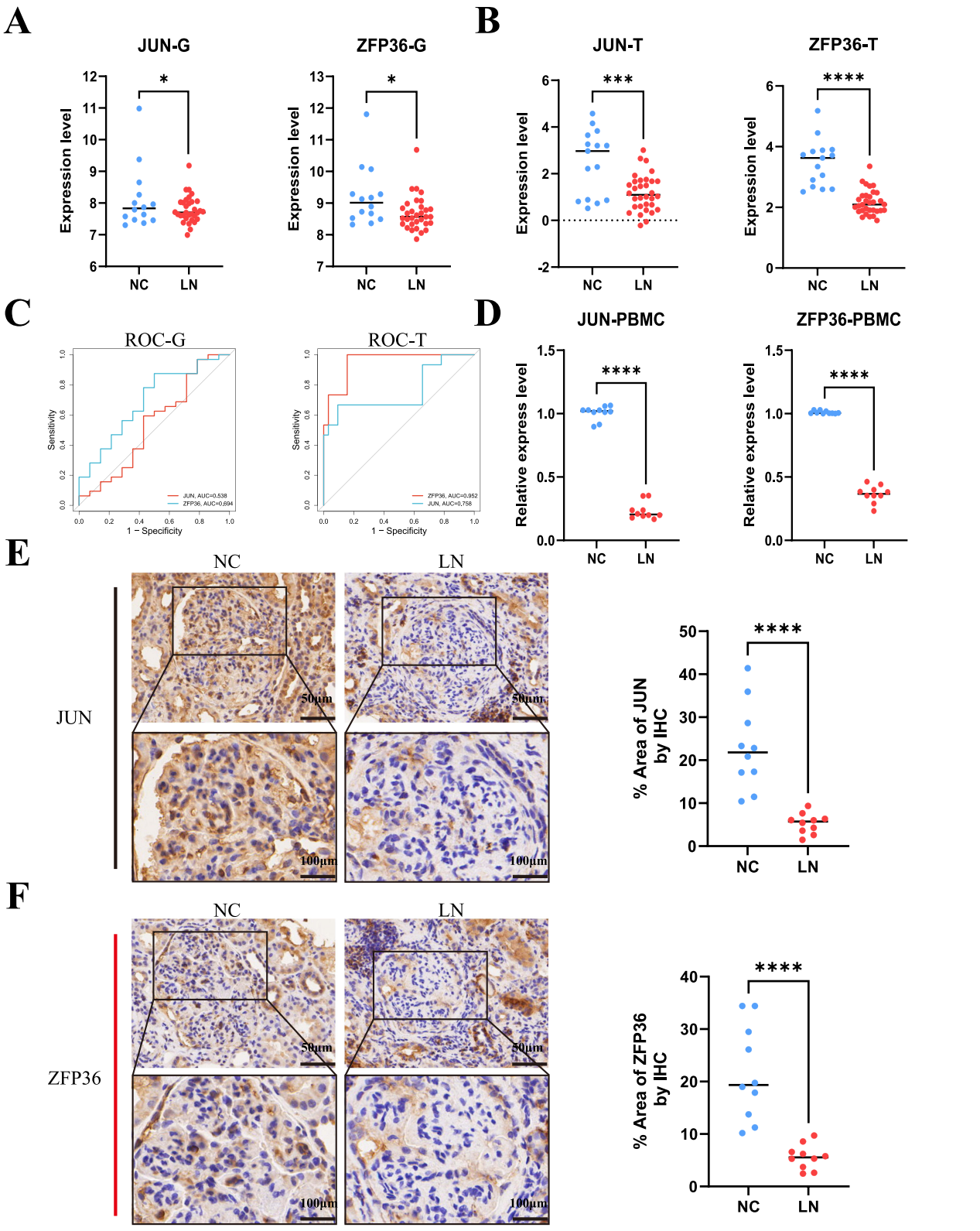

Figure 5 Validation of the hub genes in validating cohort and clinical samples. (**A**) The expression levels of hub genes in glomerular tissues in the validating cohort. (**B**) The expression levels of hub genes in renal tubule tissues in the validating cohort. (**C**) ROC curves plotted based on hub genes expression profiles in the validating cohort. (**D**) The mRNA levels of hub genes in PBMC of lupus nephritis patients and normal controls. (**E** and **F**) The expression levels of hub genes in the kidneys of lupus nephritis patients and normal controls.

Notes: **P*<0.05, ****P*<0.001, *****P*<0.0001.

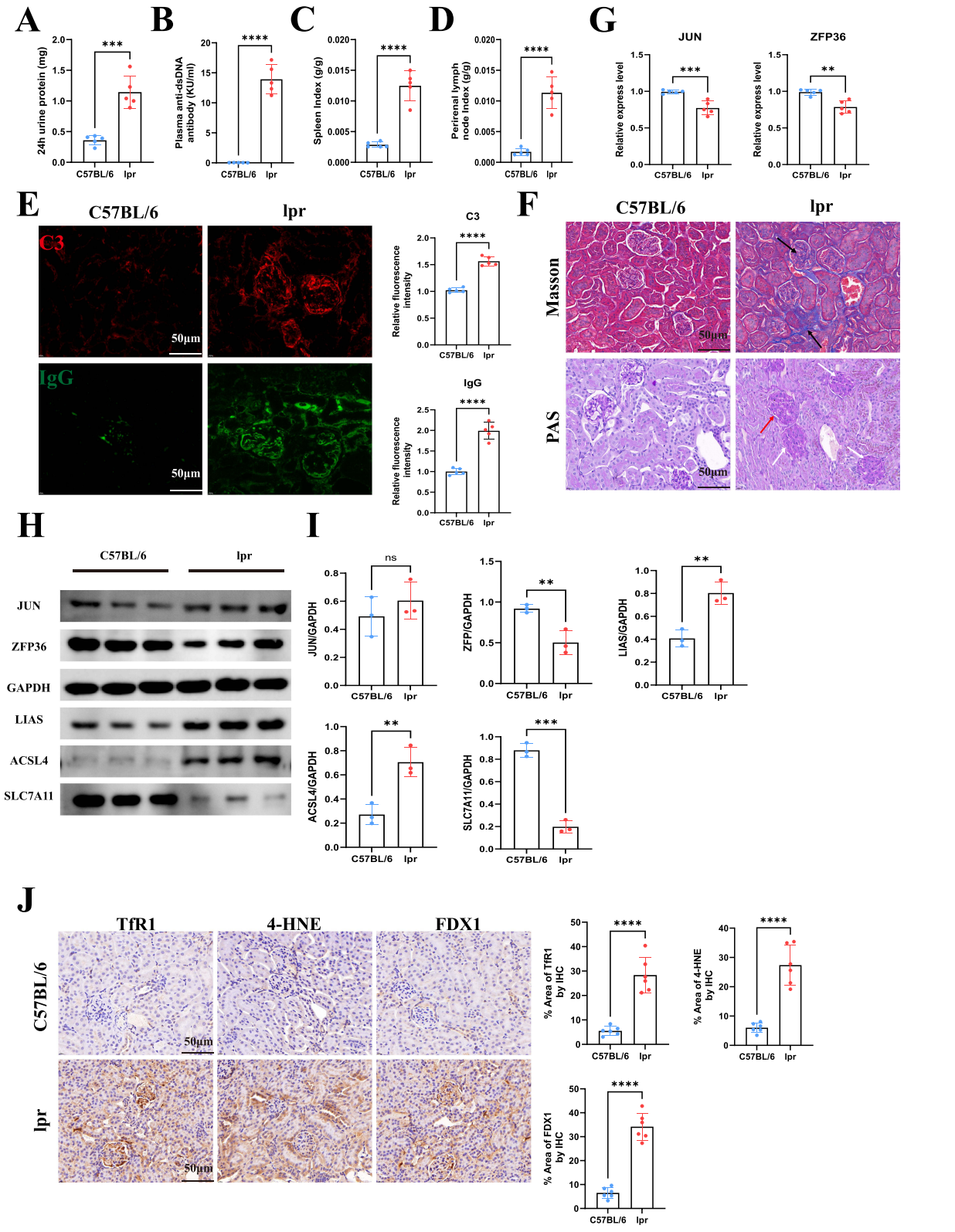

Figure 6 Animal experiments validate the expression of hub FRCGs. (**A**–**D**) The 24h urinary protein level, anti-ds-DNA antibody level, splenic index, and perirenal lymph node index in lupus mice and C57BL/6 mice. (**E**) C3 and IgG immunofluorescence staining in lupus mice and C57BL/6 mice. (**F**) Masson and PAS staining in lupus mice and C57BL/6 mice. Black arrows indicate blue areas where collagen deposition represents fibrosis. Red arrows indicate thickening of the mesangial area. White arrows indicate cellular proliferation within glomerular capillaries (mesangial cells, endothelial cells, neutrophils, etc.). (**G**) The mRNA level of the hub genes in two groups of mice. (**H** and **I**) The protein expression levels and statistical plots of hub genes, ferroptosis key genes and cuproptosis key genes in two groups of mice. (J) Protein expression levels of the ferroptosis markers TfR1 and 4HNE as well as the cuproptosis marker FDX1.

Notes: ns $P>0.05$, $^{**}P<0.01$, $^{***}P<0.001$, $^{****}P<0.0001$.

https://doi.org/10.2147/JIR.S526572

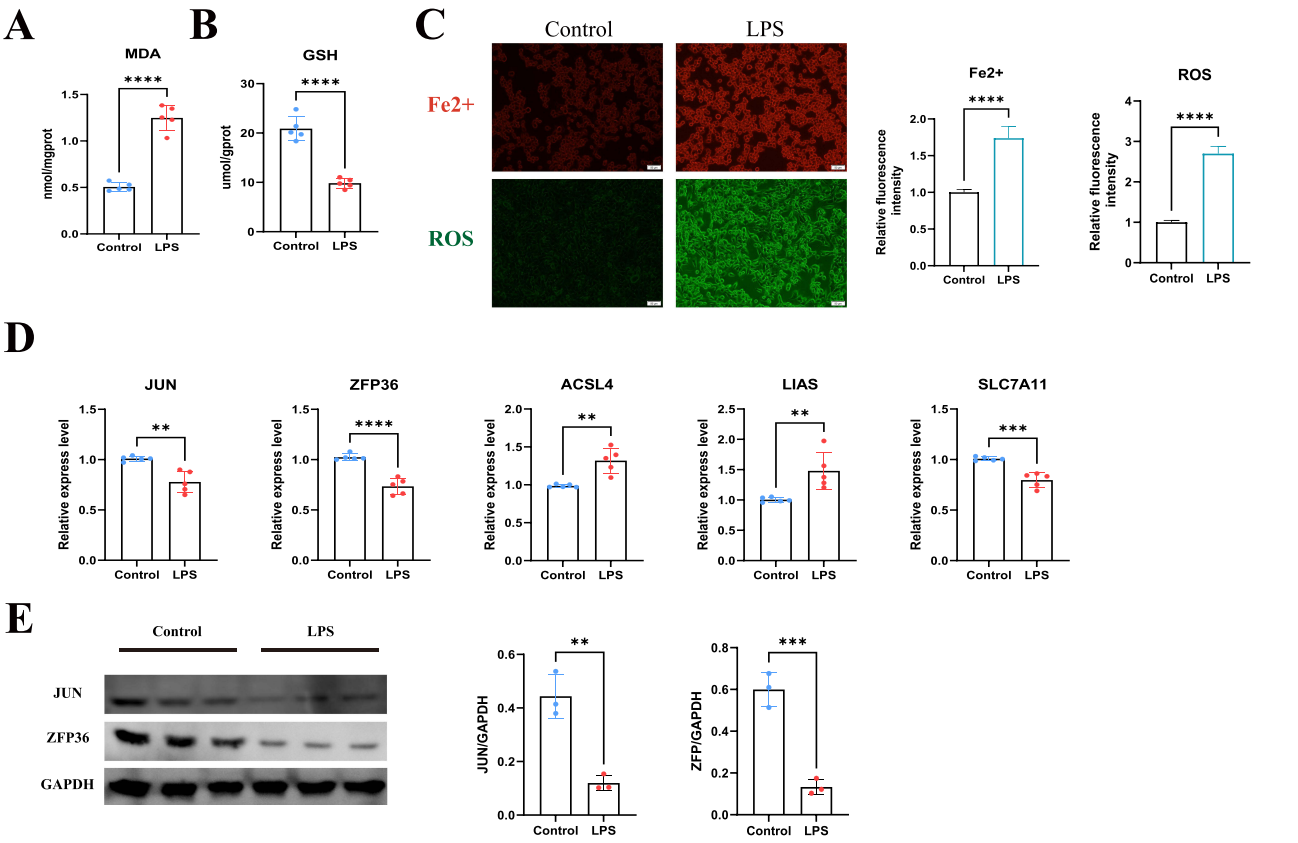

Figure 7 Cell experiments validate the expression of hub FRCGs. (**A** and **B**) MDA and GSH levels. (**C**) Representative fluorescence images and statistical plots of Fe^{2+} and ROS. (**D**) The mRNA levels of *JUN*, *ZFP36*, *ACSL4*, *LIAS* and *SLC7A11*. (**E**) The protein expression levels and statistical plots of JUN and ZFP36.
Notes: ***P*<0.01, ****P*<0.001, *****P*<0.0001.

P=0.021) and Scr levels (R= −0.66, P=0.0013, and R= −0.67, P=0.00061) (Figure 8E–H). This implied that *ZFP36* and *JUN* may alleviate the clinical symptoms of LN by inhibiting ferroptosis and cuproptosis.

Immune Infiltrate Analysis

Immune infiltration analysis revealed monocytes and macrophages as the major immune infiltrating cells in LN (Figure 9A). In LN kidneys, the expression levels of B cells naive (*P*<0.05), M1 macrophages (*P*<0.05), M2 macrophages (*P*<0.001), and monocytes (*P*<0.01) were significantly higher than those in the NC groups, whereas the expression levels of dendritic cells resting (*P*<0.01), eosinophils (*P*<0.01), and neutrophils (*P*<0.001) were significantly lower than those in the NC groups (Figure 9B). Surprisingly, *JUN* was positively correlated with neutrophils (cor= 0.64, *P*=0.002) and negatively correlated with M2 macrophages (cor= −0.51, *P*=0.018) and monocytes (cor= −0.47, *P*=0.032) (Figure 9C and D). In addition, *ZFP36* exhibited strong positive correlations with neutrophils (cor= 0.77, *P*<0.001), eosinophils (cor= 0.69, *P*<0.001), B cells memory (cor= 0.63, *P*<0.001) and T cells follicular helper (cor= 0.51, *P*=0.017), while strong negative correlations with monocytes (cor= −0.64, *P*<0.001) and M2 macrophages (cor= −0.83, *P*=0.002) (Figure 9C–E).

Discussion

In this study, we utilized bioinformatics approaches to screen 31 DE-FRCGs in the LN microarray dataset. GO functional analysis revealed that DE-FRCGs function mainly worked in response to metal ions and cellular response to oxidative stress, while KEGG enrichment analysis suggested that DE-FRCGs were mainly involved in autophagy-animal signaling pathway (hsa04140). Accumulation of iron and copper ions in the body is the initiating factor for ferroptosis and cuproptosis, while excessive oxidative stress can induce cellular ferroptosis and cuproptosis.[32,33] Furthermore, copper

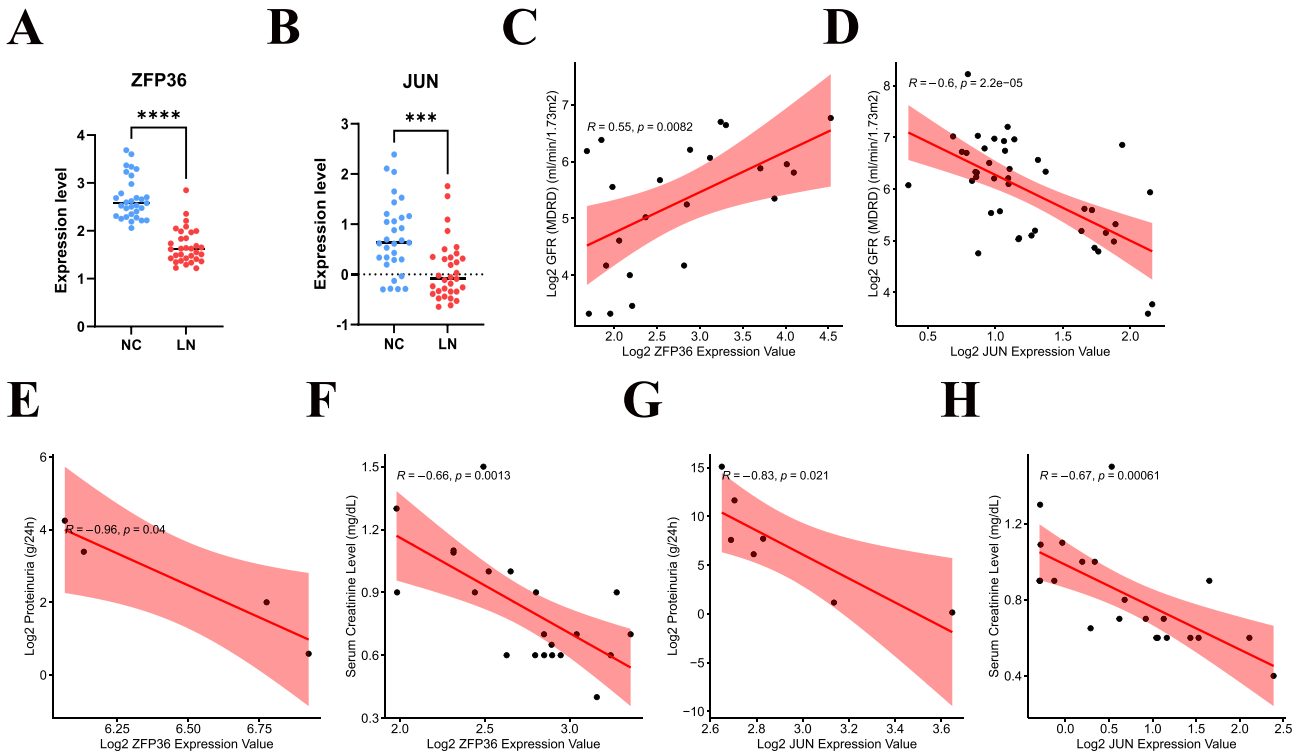

Figure 8 Correlations between hub genes and clinical traits. (**A** and **B**) The expression levels of *ZFP36* and *JUN* in the Nephroseq v5 database. (**C** and **D**) The correlation scatter plots of *ZFP36* and *JUN* with GFR. (E-H) The correlation scatter plots of *ZFP36* and *JUN* with proteinuria and Scr.
Notes: ***P<0.001, ****P<0.0001.

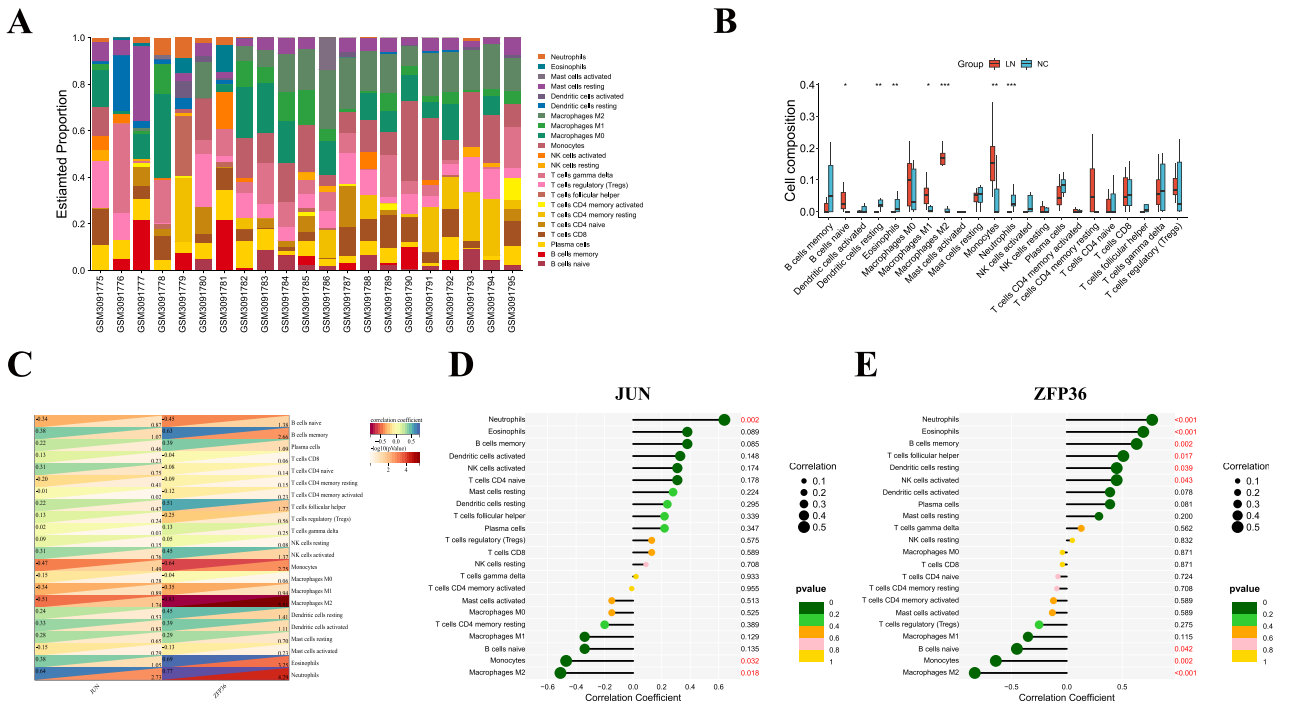

Figure 9 Analysis of immune cell infiltration in LN. (**A**) Relative percentage of immune cell subpopulations in 21 kidney samples. (**B**) Differential analysis of immune infiltrating cells between LN and NC groups. (**C**) Pearson correlation analysis of hub FRCGs in LN with immune infiltrating cells. (**D** and **E**) The lollipop charts showed the correlation between the hub genes and the immune infiltrating cells.
Notes: *P<0.05, **P<0.01, ***P<0.001.

https://doi.org/10.2147/JIR.S526572

promoted cellular ferroptosis by inducing autophagic degradation of GPX4.[13] And our previous study also detailed the relationship between autophagy and LN.[34] However, biomarkers of ferroptosis-related cuproptosis in lupus nephritis are lacking. We further screened two hub FRCGs (*JUN* and *ZFP36*) in LN using three machine learning methods and validated them with clinical samples, in vivo and in vitro experiments. Finally, immune infiltration analysis showed that they were closely associated with immune cell infiltration in LN kidney tissues.

JUN (Jun proto-oncogene, AP-1 transcription factor subunit), or c-JUN, is a functional component of the AP-1 transcription factor complex, which is often closely associated with cellular stress response, proliferation, apoptosis and cell differentiation.[35] SLE is a classic autoimmune disease triggered mainly by abnormal T-cell and B-cell interactions. In SLE, an increase in T follicular helper (TFH) and T peripheral helper (TPH) cells, which promote B-cell activation by secreting high levels of the B-cell chemokine CXCL13, is a prominent feature.[36] In contrast, type I interferon can counteract these effects and promote CXCL13 production by T cells. The aromatic hydrocarbon receptor (AHR) is a potent negative regulator of CXCL13 production by T cells. Transcriptomic and functional studies have shown that AHE acts synergistically with JUN to prevent $CXCL13^{+}$TPH/TFH cell differentiation, which serves to inhibit SLE development. In contrast, type I interferon can exacerbate SLE by disrupting the AHR-JUN axis and promoting CXCL13 secretion by T cells.[36] This is consistent with our prediction that JUN has been found to be decreased in expression in LN clinical samples, animal models, and cellular models, which may favor the onset and progression of LN. However, western blotting of JUN did not show significant differences in protein expression levels between the two groups of mice. There are several potential reasons for this inconsistency. One possibility is that the mouse model may not fully recapitulate the complex pathophysiology of lupus nephritis in humans, which could account for the lack of significant JUN expression changes. Additionally, variations in experimental conditions, such as the time point of tissue collection or the method of measurement, could also contribute to differences between the mouse and human data. Previous studies have also demonstrated that downregulation of JUN expression favors ferroptosis.[37,38] In summary, we hypothesized that downregulation of JUN may promote ferroptosis in lupus. However, reports on the relationship between JUN and cuproptosis in lupus are still lacking.

ZFP36 (Zinc finger protein 36), or tristetraprolin (TTP), is a RNA-binding protein (RBP) that induces mRNA degradation and is ubiquitous in eukaryotic organisms.[39] TTP has been implicated in the regulation of inflammatory and immune responses. TTP exerts anti-inflammatory effects by inhibiting the production of tumor necrosis factor alpha (TNF-α).[40] In addition, it is involved in neutrophil survival.[41] Recent studies have found decreased expression of RBP in peripheral blood mononuclear cells and renal biopsies of patients with LN, leading to up-regulation of the expression of inflammatory factors and exacerbation of the clinical clinical symptoms of LN.[42] Furthermore, decreased TTP mRNA expression was detected in the serum of SLE patients and was negatively correlated with disease activity.[43] These strongly support our analysis and findings. Moreover, many studies have also indicated that downregulation of ZFP36 promotes ferroptosis and cuproptosis.[44–46] Therefore, it is reasonable to hypothesize that ZFP36 plays a protective role in the development of ferroptosis and cuproptosis in lupus.

Immune cells infiltration is an essential biological feature of LN. Our analysis showed that monocytes and macrophages are the major immune infiltrating cells in LN kidneys. Macrophages drive the pro-inflammatory environment of SLE by removing dead cellular debris.[47] Meanwhile, macrophages, as an antigen-presenting cell, are able to bind to T cells, leading to T cell differentiation.[48] More importantly, macrophages can infiltrate in LN kidneys and regulate the renal immune response, thereby influencing disease progression.[49] The pro-fibrotic effect of macrophages is an important factor in the progression of LN to end-stage renal disease.[50] In addition, abnormal infiltration of monocytes in the kidney promotes renal fibrosis.[51] Wang et al found that dysregulation of monocytes was also positively correlated with SLE activity.[52] The two hub genes (*JUN* and *ZFP36*) were negatively correlated with monocytes and macrophages, suggesting that low expression of hub genes in LN may favor infiltration of monocytes and macrophages in LN kidneys to aggravate renal inflammation and injury.

There are also several limitations in this study. Firstly, the microarray data in this study were obtained from publicly available databases and were secondary mined from existing data, which may have false positives. Secondly, while our integrated machine learning model demonstrated perfect discrimination in the training cohort (AUC=1.000), this likely reflects overfitting attributable to the limited sample size (n=21). Multi-omics integration or longitudinal datasets could be considered in the future to address sample size and mechanistic gaps in future studies. Thirdly, while our study compared LN against healthy controls to identify disease-associated signatures, future studies should include positive

controls (eg, IgA nephropathy, diabetic nephropathy) to rigorously evaluate the specificity of hub FRCGs for LN versus other renal pathologies. Finally, the mechanisms by which hub genes regulate ferroptosis and cuproptosis in the LN need to be investigated in greater depth by additional in vitro and in vivo experiments.

Conclusion

In conclusion, we identified two hub ferroptosis-related cuproptosis genes (*JUN* and *ZFP36*) in LN and confirmed their reduced expression in LN. Moreover, the low expression of the hub genes may increase the level of monocyte and macrophage infiltration aggravating renal injury. *JUN* and *ZFP36* may be good biomarkers for lupus nephritis.

Data Availability Statement

The datasets generated and/or analysed during the current study are available in the [GEO] repository, [https://www.ncbi.nlm.nih.gov/geo/query/acc.cgi?acc=GSE112943].

Acknowledgments

Su Zhang and Weitao Hu are co-first authors in this work. We thank all those who participated in this study.

Funding

This work was supported by the Natural Science Foundation of Fujian Province (Grant number: 2024J01686) and the Joint funds for the innovation of science and technology, Fujian province (Grant number: 2023Y9236).

Disclosure

The authors declare no competing interests in this work.

References

1. Zou M, Qian D, Luo R, Cheng Y, Xu G, Ge S. Identifying potential mechanism and targets for treatment of tertiary lymphoid structure in lupus nephritis based on bioinformatics analysis. *Int Immunopharmacol*. 2025;148:114084. doi:10.1016/j.intimp.2025.114084
2. Lichtnekert J, Anders HJ. Lupus nephritis-related chronic kidney disease. *Nat Rev Rheumatol*. 2024;20(11):699–711. doi:10.1038/s41584-024-01158-w
3. Hoi A, Igel T, Mok CC, Arnaud L. Systemic lupus erythematosus. *Lancet*. 2024;403(10441):2326–2338. doi:10.1016/S0140-6736(24)00398-2
4. Yu C, Li P, Dang X, Zhang X, Mao Y, Chen X. Lupus nephritis: new progress in diagnosis and treatment. *J Autoimmun*. 2022;132:102871. doi:10.1016/j.jaut.2022.102871
5. Dixon SJ, Lemberg KM, Lamprecht MR, et al. Ferroptosis: an iron-dependent form of nonapoptotic cell death. *Cell*. 2012;149(5):1060–1072. doi:10.1016/j.cell.2012.03.042
6. Jiang X, Stockwell BR, Conrad M. Ferroptosis: mechanisms, biology and role in disease. *Nat Rev Mol Cell Biol*. 2021;22(4):266–282. doi:10.1038/s41580-020-00324-8
7. Wlazlo E, Mehrad B, Morel L, Scindia Y. Iron metabolism: an under investigated driver of renal pathology in lupus nephritis. *Front Med*. 2021;8:643686. doi:10.3389/fmed.2021.643686
8. Li P, Jiang M, Li K, et al. Glutathione peroxidase 4-regulated neutrophil ferroptosis induces systemic autoimmunity. *Nat Immunol*. 2021;22(9):1107–1117. doi:10.1038/s41590-021-00993-3
9. Marks ES, Bonnemaison ML, Brusnahan SK, et al. Renal iron accumulation occurs in lupus nephritis and iron chelation delays the onset of albuminuria. *Sci Rep*. 2017;7(1):12821. doi:10.1038/s41598-017-13029-4
10. Kahlson MA, Dixon SJ. Copper-induced cell death. *Science*. 2022;375(6586):1231–1232. doi:10.1126/science.abo3959
11. Yang L, Yang P, Lip GYH, Ren J. Copper homeostasis and cuproptosis in cardiovascular disease therapeutics. *Trends Pharmacol Sci*. 2023;44(9):573–585. doi:10.1016/j.tips.2023.07.004
12. Chen L, Min J, Wang F. Copper homeostasis and cuproptosis in health and disease. *Sign Transduc Targe Therapy*. 2022;7(1):378. doi:10.1038/s41392-022-01229-y
13. Xue Q, Yan D, Chen X, et al. Copper-dependent autophagic degradation of GPX4 drives ferroptosis. *Autophagy*. 2023;19(7):1982–1996. doi:10.1080/15548627.2023.2165323
14. Clough E, Barrett T, Wilhite SE, et al. NCBI GEO: archive for gene expression and epigenomics data sets: 23-year update. *Nucleic Acids Res*. 2024;52(D1):D138–d144. doi:10.1093/nar/gkad965
15. Ritchie ME, Phipson B, Wu D, et al. limma powers differential expression analyses for RNA-sequencing and microarray studies. *Nucleic Acids Res*. 2015;43(7):e47. doi:10.1093/nar/gkv007
16. Langfelder P, Horvath S. WGCNA: an R package for weighted correlation network analysis. *BMC Bioinf*. 2008;9(1):559. doi:10.1186/1471-2105-9-559
17. Zhou N, Yuan X, Du Q, et al. FerrDb V2: update of the manually curated database of ferroptosis regulators and ferroptosis-disease associations. *Nucleic Acids Res*. 2023;51(D1):D571–d582. doi:10.1093/nar/gkac935

18. Safran M, Dalah I, Alexander J, et al. GeneCards version 3: the human gene integrator. *Database*. 2010;2010:baq020. doi:10.1093/database/baq020
19. Liberzon A, Birger C, Thorvaldsdóttir H, Ghandi M, Mesirov JP, Tamayo P. The molecular signatures database (MSigDB) hallmark gene set collection. *Cell Systems*. 2015;1(6):417–425. doi:10.1016/j.cels.2015.12.004
20. Tsvetkov P, Coy S, Petrova B, et al. Copper induces cell death by targeting lipoylated TCA cycle proteins. *Science*. 2022;375(6586):1254–1261. doi:10.1126/science.abf0529
21. Szklarczyk D, Kirsch R, Koutrouli M, et al. The STRING database in 2023: protein-protein association networks and functional enrichment analyses for any sequenced genome of interest. *Nucleic Acids Res*. 2023;51(D1):D638–d646. doi:10.1093/nar/gkac1000
22. Doncheva NT, Morris JH, Holze H, et al. Cytoscape stringApp 2.0: analysis and visualization of heterogeneous biological networks. *J Proteome Res*. 2023;22(2):637–646. doi:10.1021/acs.jproteome.2c00651
23. Wu T, Hu E, Xu S, et al. clusterProfiler 4.0: a universal enrichment tool for interpreting omics data. *Innovation*. 2021;2(3):100141. doi:10.1016/j.xinn.2021.100141
24. Friedman J, Hastie T, Tibshirani R. Regularization paths for generalized linear models via coordinate descent. *Journal of Statistical Software*. 2010;33(1):1–22. doi:10.18637/jss.v033.i01
25. Rigatti SJ. Random Forest. *J Insur Med*. 2017;47(1):31–39.
26. Sanz H, Valim C, Vegas E, Oller JM, Reverter F. SVM-RFE: selection and visualization of the most relevant features through non-linear kernels. *BMC Bioinf*. 2018;19(1):432. doi:10.1186/s12859-018-2451-4
27. Robin X, Turck N, Hainard A, Tiberti N, Lisacek F, Sanchez JC. Müller M: pROC: an open-source package for R and S+ to analyze and compare ROC curves. *BMC Bioinf*. 2011;12(1):77. doi:10.1186/1471-2105-12-77
28. Zhang S, Hu W, Tang Y, Lin H, Chen X. Identification of hub immune-related genes and construction of predictive models for systemic lupus erythematosus by bioinformatics combined with machine learning. *Front Med*. 2025;12:1557307. doi:10.3389/fmed.2025.1557307
29. Wen Q, Wang C, Chen D, et al. Proteomics-based identification of potential therapeutic targets of artesunate in a lupus nephritis MRL/lpr mouse model. *J Proteome Res*. 2024;23(4):1150–1162. doi:10.1021/acs.jproteome.3c00558
30. Sundararaj K, Rodgers J, Angel P, Wolf B, Nowling TK. The role of neuraminidase in TLR4-MAPK signalling and the release of cytokines by lupus serum-stimulated mesangial cells. *Immunology*. 2021;162(4):418–433. doi:10.1111/imm.13294
31. Newman AM, Liu CL, Green MR, et al. Robust enumeration of cell subsets from tissue expression profiles. *Nature Methods*. 2015;12(5):453–457. doi:10.1038/nmeth.3337
32. Panda SK, Peng V, Sudan R, et al. Repression of the aryl-hydrocarbon receptor prevents oxidative stress and ferroptosis of intestinal intraepithelial lymphocytes. *Immunity*. 2023;56(4):797–812.e794. doi:10.1016/j.immuni.2023.01.023
33. Zhang Y, Zhang N, Xing J, et al. In situ hydrogel based on Cu-Fe(3)O(4) nanoclusters exploits oxidative stress and the ferroptosis/cuproptosis pathway for chemodynamic therapy. *Biomaterials*. 2024;311:122675. doi:10.1016/j.biomaterials.2024.122675
34. Zhang S, Hu W, Tang Y, Chen X. Identification and validation of key autophagy-related genes in lupus nephritis by bioinformatics and machine learning. *PloS one*. 2025;20(1):e0318280. doi:10.1371/journal.pone.0318280
35. Scopa C, Barnada SM, Cicardi ME, Singer M, Trotti D, Trizzino M. JUN upregulation drives aberrant transposable element mobilization, associated innate immune response, and impaired neurogenesis in Alzheimer's disease. *Nat Commun*. 2023;14(1):8021. doi:10.1038/s41467-023-43728-8
36. Law C, Wacleche VS, Cao Y, et al. Interferon subverts an AHR-JUN axis to promote CXCL13(+) T cells in lupus. *Nature*. 2024;631(8022):857–866.
37. Cao W, Li Y, Zeng Z, Lei S. Terpinen-4-ol induces ferroptosis of glioma cells via downregulating JUN proto-oncogene. *Molecules*. 2023;28(12):4643. doi:10.3390/molecules28124643
38. Gao D, Huang Y, Sun X, Yang J, Chen J, He J. Overexpression of c-Jun inhibits erastin-induced ferroptosis in Schwann cells and promotes repair of facial nerve function. *J Cell & Mol Med*. 2022;26(8):2191–2204. doi:10.1111/jcmm.17241
39. Snyder BL, Blackshear PJ. Clinical implications of tristetraprolin (TTP) modulation in the treatment of inflammatory diseases. *Pharmacol Ther*. 2022;239:108198. doi:10.1016/j.pharmthera.2022.108198
40. Kovarik P, Bestehorn A, Fesselet J. Conceptual advances in control of inflammation by the RNA-binding protein tristetraprolin. *Front Immunol*. 2021;12:751313. doi:10.3389/fimmu.2021.751313
41. Ebner F, Sedlyarov V, Tasciyan S, et al. The RNA-binding protein tristetraprolin schedules apoptosis of pathogen-engaged neutrophils during bacterial infection. *J Clin Invest*. 2017;127(6):2051–2065. doi:10.1172/JCI80631
42. Fakhfakh R, Bouallegui E, Houssaini H, et al. Differential expression of anti-inflammatory RNA binding proteins in lupus nephritis. *Life*. 2022;12(10):1474. doi:10.3390/life12101474
43. Rizk SK, Alhosary A, Zahran ES, Awad S, Khalil M. Identification of potential biomarkers for SLE through mRNA expression profiling. *J Immunoassay Immunochem*. 2024;45(1):20–37. doi:10.1080/15321819.2023.2266013
44. Zhang Z, Guo M, Li Y, et al. RNA-binding protein ZFP36/TTP protects against ferroptosis by regulating autophagy signaling pathway in hepatic stellate cells. *Autophagy*. 2020;16(8):1482–1505. doi:10.1080/15548627.2019.1687985
45. Li X, Hu Y, Wu Y, Yang Z, Liu Y, Liu H. Exosomal let-7a-5p derived from human umbilical cord mesenchymal stem cells alleviates coxsackievirus B3-induced cardiomyocyte ferroptosis via the SMAD2/ZFP36 signal axis. *J Zhejiang Univ Sci B*. 2024;25(5):422–437. doi:10.1631/jzus.B2300077
46. Zhang M-J, Shi M, Yu Y, Ou R, Ge R-S, Duan P. Curcuminoid PBPD induces cuproptosis and endoplasmic reticulum stress in cervical cancer via the Notch1/RBP-J/NRF2/FDX1 pathway. *Molecular Carcinogenes*. 2024;63(8):1449–1466. doi:10.1002/mc.23735
47. Yoo EJ, Oh KH, Piao H, et al. Macrophage transcription factor TonEBP promotes systemic lupus erythematosus and kidney injury via damage-induced signaling pathways. *Kidney Int*. 2023;104(1):163–180. doi:10.1016/j.kint.2023.03.030
48. Burbano C, Villar-Vesga J, Vásquez G, Muñoz-Vahos C, Rojas M, Castaño D. Proinflammatory differentiation of macrophages through microparticles that form immune complexes leads to T- and B-cell activation in systemic autoimmune diseases. *Front Immunol*. 2019;10:2058. doi:10.3389/fimmu.2019.02058
49. Meng XM, Tang PM, Li J, Lan HY. Macrophage phenotype in kidney injury and repair. *Kidney Diseases*. 2015;1(2):138–146. doi:10.1159/000431214
50. Tang PM, Nikolic-Paterson DJ, Lan HY. Macrophages: versatile players in renal inflammation and fibrosis. *Nat Rev Nephrol*. 2019;15(3):144–158. doi:10.1038/s41581-019-0110-2

51. Vegting Y, Jongejan A, Neele AE, et al. Infiltrative classical monocyte-derived and SPP1 lipid-associated macrophages mediate inflammation and fibrosis in ANCA-associated glomerulonephritis. *Nephrol Dialysis Transpl*. 2024;2024:1.
52. Wang Z, Yang C, Gao W, et al. Systemic lupus erythematosus-specific CD14(+)IFITM3(+) monocyte: implications for disease activity and progression. *Int Immunopharmacol*. 2025;146:113916. doi:10.1016/j.intimp.2024.113916